# Anisotropic effects in elastic and incipient plastic deformation under (001), (110), and (111) nanoindentation of Al and Cu

T. Tsuru[1] and Y. Shibutani[1,2]
[1]*Department of Mechanical Engineering, Osaka University, Osaka, Japan*
[2]*Center for Atomic and Molecular Technologies, Osaka University, Osaka, Japan*
(Received 21 September 2006; revised manuscript received 8 November 2006; published 16 January 2007)

Atomistic simulations of (001), (110), and (111) nanoindentation are performed to investigate anisotropic effects in elastic and incipient plastic behavior under nanoindentation. We compared two materials, single-crystalline Al and Cu, focusing on the large difference between their anisotropic properties. The indent load-depth behavior of Al during elastic deformation exhibits slight anisotropy, while that of Cu varies greatly according to the indentation axis. In addition, incipient plastic deformation, that is, dislocation nucleation, depends largely on the predicted slip system. While dislocations are emitted on the surface when indented by a spherical indenter with small radius, collective dislocation emission occurs from within the material. In the case of dislocation emission within the material, the critical mean pressure, which is an important indicator of dislocation nucleation, is inherent to the indentation axis in both materials.

DOI: 10.1103/PhysRevB.75.035415 PACS number(s): 61.72.Lk, 62.20.Fe, 31.15.Qg

## I. INTRODUCTION

Recent advances in material miniaturization and high-accuracy measurement techniques have allowed us to measure the mechanical properties of nanoscale materials. Nanoindentation has been widely used because of its applicability under ambient conditions.[1,2] In the last decade, numerous studies have employed nanoindentation to test a variety of different materials, helping to identify characteristic phenomena, as well as determine material properties. One phenomenon that is unique to nanoscale materials is the so-called displacement burst, which is the abrupt increase in indent depth following homogeneous elastic deformation observed in crystalline materials.[3–6] Many models, such as the prismatic dislocation model,[5] geometrically necessary dislocation model,[7,8] and Frank-Read source model,[9] have been proposed to explain this nonlinear phenomenon. These models suggest that displacement burst is caused by collective dislocation nucleation.

While experimental nanoindentation tests have achieved significant results in nanoscale properties, we need to recognize that material properties measured by nanoindentation are generally evaluated according to contact mechanics of isotropic elastic bodies. For instance, if the material under investigation is indented by a spherical indenter, a Hertzian elastic solution is applied to evaluate its elastic properties. This approach is widely used and yields reasonable results in certain cases. However, the assumption of isotropy may lead to critical errors in the case of metals and materials with strongly anisotropic structures. Kiely and Houston conducted nanoindentation in single crystalline Au with different axes to investigate the effect of anisotropy, and showed the differences in indentation behavior caused by varying the indentation axis.[10] Thus, anisotropy is said to be a complicating factor in nanoindentation measurement.

## II. ANALYSIS MODEL AND BASIC PHYSICAL PROPERTIES

Atomic scale simulations such as molecular dynamics can be effective tools because they can directly treat an explicit expression of structural anisotropy and the yield process at the atomic level. While the numerous atomistic simulations that have been analyzed have provided useful insight into dislocation nucleation and crystallographic analysis,[11–14] there is a lack of information on the problems caused by anisotropic effects. In the present paper, we perform atomistic simulations of nanoindentation on three different surfaces of (001), (110), and (111) planes to elucidate anisotropic effects on elastic deformation and dislocation nucleation under nanoindentation. We chose single-crystalline Al and Cu as our test materials since these have quite different anisotropic factors. Atomic models of Al and Cu are three-dimensional cubic, containing approximately 500 000 atoms in sizes of 20 and 18 nm, respectively. In some cases, larger models containing up to $2\times10^6$ atoms are used also in order to consider the size dependence. Coordinate systems are taken as $x[100]$, $y[010]$, $z[001]$ for (001) indentation, $x'[111]$, $y'[11\bar{2}]$, $z'[\bar{1}10]$ for (110), and $x''[\bar{1}10]$, $y''[\bar{1}\,\bar{1}2]$, $z''[111]$ for (111), where the indentation axes of all models are set to the $z$ direction. The top surface is traction-free and atoms located on the bottom surface are absolutely fixed. Periodic boundary conditions are applied in the direction perpendicular to the indentation axis. An embedded atom method (EAM) type of interatomic potential proposed by Mishin *et al.*[15,16] is employed to express the interaction of Al or Cu atoms, and the repulsive potential by Kelchner *et al.*[17] is used to simulate the frictionless contact between the atomic model and spherical rigid indenter. Indentation is simulated for three different indenter radii, namely, $r5$, $r15$, and $r30$ nm, as well as three different indentation planes. All simulations are performed as a quasistatic analysis under absolute temperature (0 K) by the conjugate gradient (CG) method. Indent load is applied in small increments of indent depth ($\sim$0.025 nm) and a fully relaxed condition is obtained by sufficient CG relaxation. A set of calculations is reiterated until the indent depth reaches a maximum depth. The indentation behavior is characterized through the basic physical properties shown in Table I. The anisotropic factor can be evaluated by the following relation:

 

TABLE I. Physical properties of Al and Cu predicted by Mishin *et al.* potential (Ref. 15) compared with the experimental results or density functional theory (DFT).

| | Al | | Cu | |
|---|---|---|---|---|
| | Ref. 15 | Expt. or DFT | Ref. 15 | Expt. or DFT |
| | | Elastic constant (GPa) | | |
| $C_{11}$ | 114 | 114[a] | 169.9 | 170.0[a] |
| $C_{12}$ | 61.5 | 61.9[a] | 122.6 | 122.5[a] |
| $C_{44}$ | 31.6 | 31.6[a] | 76.2 | 75.8[a] |
| | | Anisotropic factor[b] | | |
| $\alpha$ | 1.20 | 1.21 | 3.22 | 3.19 |
| | | Stacking fault energy ($mJ/m^2$) | | |
| $\gamma_{SF}$ | 156.6 | 158[c] | 44.7 | 39[c] |

[a]Reference 18.
[b]Calculated by Eq. (1).
[c]Reference 19.

$$\alpha = \frac{2C_{44}}{C_{11} - C_{12}}. \quad (1)$$

As can be seen from Table I, Al and Cu differ significantly in anisotropic factor and stacking fault energy.

## III. RESULTS AND DISCUSSION

The relationship between indent load and depth for indenters of varying radius on three different planes is shown in Fig. 1. Here, three different planes in Al and Cu are indented by spherical indenters having three different radii.

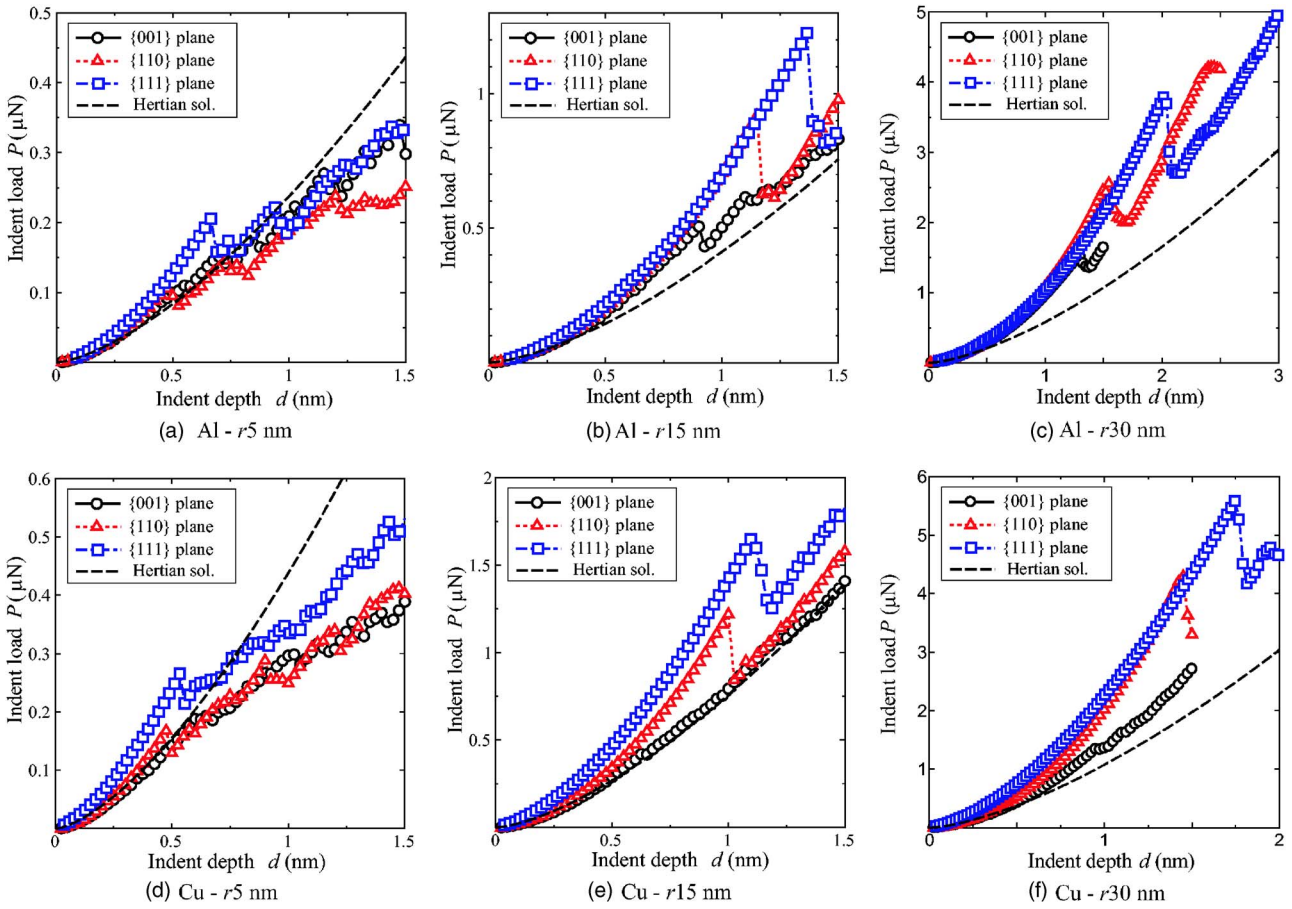


FIG. 1. (Color online) Relationship between indent load and depth for three spherical indenters having different radii and three different indentation axes and the elastic solution.

TABLE II. Elastic properties calculated under the assumption of uniaxial tension.

| | $E'$ (GPa) | $\nu'$ | $E^*$ (GPa) |
|---|---|---|---|
| Al (001) | 70.6 | 0.351 | 80.5 |
| Al (110) | 80.4 | 0.331 | 90.3 |
| Al (111) | 83.6 | 0.324 | 93.4 |
| Cu (001) | 67.1 | 0.419 | 81.4 |
| Cu (110) | 163 | 0.302 | 179 |
| Cu (111) | 193 | 0.294 | 211 |

The Hertzian elastic solutions,[20] which can be obtained via $P=(4/3)E^*R^{1/2}d^{3/2}$, are also shown for all cases. Here, $R$ is the radius of the spherical indenter, $d$ is the indent depth, and $E^*$ is the reduced indentation modulus, represented by the Young's modulus and Poisson's ratio of the specimen and indenter.[20] In the present study, we assume that the indenter is ideally rigid, and thus the reduced modulus is given by $E^*=E_s/(1-\nu_s^2)$. We obtain a Hertzian solution when $E^*=80.1$ and 147.1 GPa in Al and Cu, respectively, where the Young's modulus and Poisson's ratio can be found in Ref. 21, and those are determined based on the polycrystalline average. In Fig. 1, abrupt drops in load, indicative of dislocation nucleation, are observed after continuous elastic deformation. When we focus on anisotropic effects in Al and Cu during elastic deformation, we find that the $P$-$d$ relationship in the case of Al [Figs. 1(a)–1(c)] is almost constant, while that in Cu [Figs. 1(d)–1(f)] varies with indentation direction. In particular, (110) and (111) indentations in Cu exhibit greater loads than (001) indentation. These differences are due to anisotropic effects. Thus, we attempt to estimate these effects by using the Hertzian relationship presented above. In the case of uniaxial tension, the Young's modulus and Poisson's ratio can be obtained by anisotropic elastic constants via the following relations: $E'=(C_{11}-C_{12})\times(C_{11}+2C_{12})/(C_{11}+C_{12})$, $\nu'=C_{12}/(C_{11}+C_{12})$. Thus, we evaluated the reduced modulus for each direction by applying the above relationships and the Voigt approximation. The coefficients $E$, $\nu$, and $E^*$ obtained using the Mishin *et al.* potential are shown in Table II, where the anisotropic elastic constants for each tensile axis are obtained by proper orthogonal rotation. Reduced moduli for Al vary little with direction, while a marked variation is observed in the case of Cu. Since indent load $P$ is proportional to the reduced modulus, these evaluations provide a qualitative explanation for the anisotropic effects during elastic deformation illustrated in Fig. 1. To obtain a better understanding, we show distributions of the von Mises equivalent stress under the indenter tip in Al and Cu in Fig. 2, where all snapshots are taken at the same indent depth ($d$=0.5 nm) when indented by $r$15 nm indenter. These images were created by the visualization software ATOMEYE.[22] Each indentation direction has a different overall distribution shape and scale in both materials. This scale difference is associated with the indentation properties shown in Table II. In addition to the variation with indentation direction, differences between materials are confirmed, especially in the case of (001) indentation. Al shows

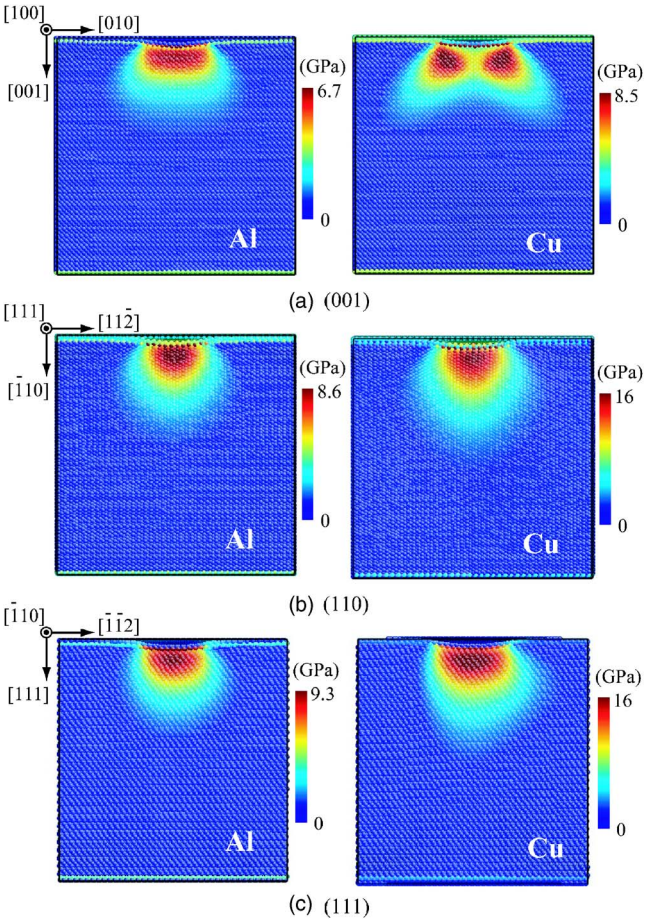


FIG. 2. (Color online) Distributions of von Mises equivalent stress for (001), (110), and (111) indentation in Al and Cu.

a shape similar to that of the isotropic elastic solution,[20] while Cu with a larger anisotropic factor shows a dramatic anisotropic effect. This anisotropic effect has a direct influence on the location of maximum shear stress associated with dislocation nucleation.[23]

In our previous study, we noted that the mean pressure is one of the most important indicators of dislocation nucleation because the relationship between maximum shear stress and mean pressure is linear even in anisotropic media.[23] In the present study, the mean pressure shown in Fig. 3 is defined as $p_m=P/A_c$, where $A_c$ is the contact area calculated directly in the relaxed condition. It appears in Fig. 3 that most of the planes have their own critical mean pressure $p_c$, which denotes dislocation nucleation. In some cases, however, it is difficult to estimate a specific critical mean pressure for each plane. In concrete terms, Figs. 3(a), Al(001) $r5$, and 3(d), Cu(001) $r5$, represent unstable behavior, Fig. 3(b), Al(110) $r5$, shows a smaller critical value than the other indenters, and each indenter in Fig. 3(e), Cu(110), shows a completely different value. Unstable behavior when indented using a small radius of the indenter as shown in Figs. 3(a), Al(001) $r5$, and 3(d), Cu(001) $r5$, is derived from heterogeneous deformation of the top surface. In addition, surface defects can be generated before dislocation emission. And there is an additional contributing factor in (110) indentation by a small radius of indenter as described below. Omitting

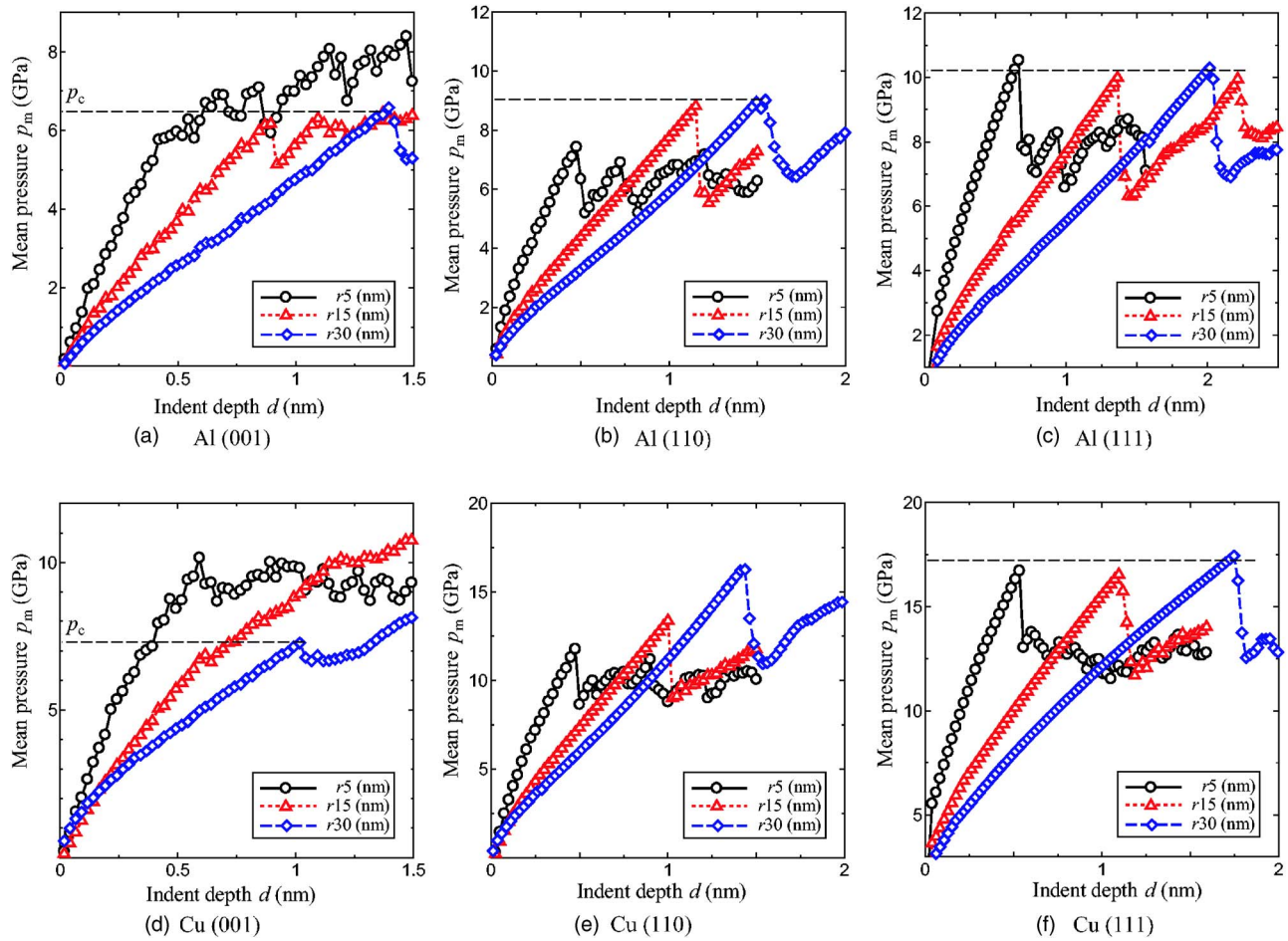


FIG. 3. (Color online) Relationship between mean pressure and depth during indentation on three different planes by three spherical indenters, each having a different radius.

the case of small radius, we can estimate the critical mean pressure for (100) and (111) indentation, and confirm that $p_c^{(111)}$ (10.2 GPa in Al, 17.0 GPa in Cu) is much larger than $p_c^{(001)}$ (6.5 GPa in Al, 7.4 GPa in Cu). For the sake of comparison, we again assumed uniaxial tension, and evaluated the Schmid factor for each tensile axis in Table III. Here, the number of activated slip planes, $n_a$, the angle between the tensile axis and primary slip plane, $\theta$, and the Schmid factors of $\langle 110 \rangle$ and $\langle 11\bar{2} \rangle$ slip directions, $s_{\langle 110 \rangle}$ and $s_{\langle 11\bar{2} \rangle}$ are shown. Clearly, the (111) indentation needs a larger applied load to reach the critical resolved shear stress compared to the other directions. These crystallographic evaluations of the Schmid factor and reduced modulus provide a direct explanation for the differences between (001) and (111).

Figure 4 shows the dislocation emission and predicted slip systems associated with Table III under nanoindentation on three different planes in Al and Cu. Also shown in this figure is the pattern diagram of the activated slip system associated with the Thompson tetrahedron under each plane. We visualize the defect structures on the basis of a potential energy criterion specifying only the atoms that have an energy above −3.33 eV in Al and −3.50 eV in Cu. Figure 4 confirms that dislocations are emitted on the predicted slip system under (001) and (111) indentation, though not all slip systems are necessarily activated. In addition, surface defects can be certainly observed in the case that the $r$5 nm indenter is used, and these surface defects have a large impact on the indent load and mean pressure.

TABLE III. Schmid factors for the three tensile axes and two slip directions.

| Tensile axis | $n_a$ | $\theta$ (deg) | $s_{\langle 110 \rangle}$ | $s_{\langle 11\bar{2} \rangle}$ |
|---|---|---|---|---|
| $\langle 100 \rangle$ | 8 | 54.74 | 0.4082 | 0.4714 |
| $\langle 110 \rangle$ | 4 | 35.26 | 0.4082 | 0.4714 |
| $\langle 111 \rangle$ | 6 | 70.53 | 0.2722 | 0.1571 |

Emitted dislocations produced within the material immediately interact with other dislocations on the adjacent slip plane, and subsequently form prismatic dislocations. At first glance, these interactions seem to create sessile dislocation locks, but they never cause immobilization of dislocations. We have reached this conclusion after detailed analysis of activated slip systems under nanoindentation and the nanoinclusion problem and confirming that all interactions are crystallographically equivalent and energetically unfavorable.[23,24] In the case of (110) indentation, the patterns of dislocation emission vary with the radius of the spherical indenter. When (110) indentation is conducted using a small indenter radius, the slip system parallel to the indentation axis is activated, and dislocation nucleation occurs from the

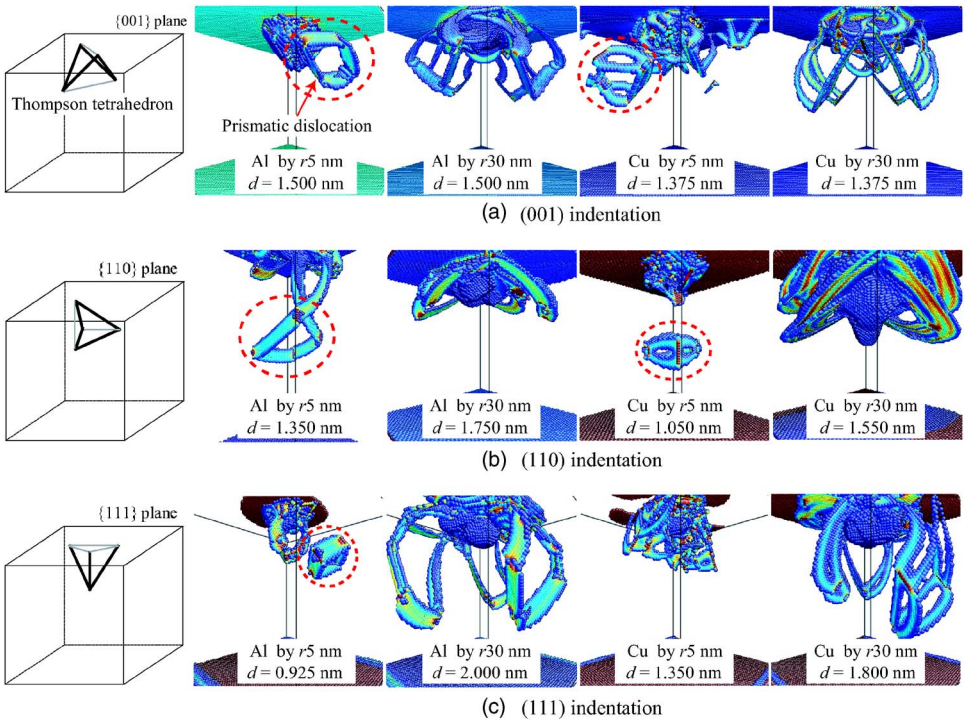


FIG. 4. (Color online) Dislocation emission under (001), (110), and (111) nanoindentation by $r5$ and $r30$ nm indenters, and diagrams of the activated slip systems (bold line) associated with Thompson tetrahedron.

surface. Thus the critical pressure value is not constant in this particular case. However, when dislocation nucleation occurs within the material, the critical mean pressure is constant, determined solely by the indentation plane.

## IV. CONCLUSIONS

In conclusion, we have performed atomistic simulations of (001), (110), and (111) nanoindentation in Al and Cu with spherical indenters of varying radius to investigate anisotropic effects on the elastic and incipient yield event under nanoindentation. Cu, which has a much larger anisotropic factor than Al, shows a marked anisotropic behavior in terms of the load-depth relation and stress distribution. In particular, the reduced modulus in the case of (111) indentation is twice that in the case of (001) indentation. In addition, we found that (001) and (111) exhibit an inherent critical mean pressure for dislocation nucleation, while (110) shows values that vary according to the indenter radius, caused by variations in the location of dislocation emission. More specifically, the critical mean pressure is intrinsically constant when dislocation nucleation occurs within the material.

Finally, particular attention should be given to anisotropic effects in the nanoindentation measurement of polycrystalline solids, because each crystal grain that constructs a polycrystalline solid has its own directional property to the indentation axis, and average characteristics of the whole system of the polycrystal can no longer be applied to the nanoscale measurement.

## ACKNOWLEDGMENTS

This work was supported by a Grant-in-Aid from JSPS (Grant No. 179504).

[1] G. M. Pharr, W. C. Oliver, and F. R. Brontzen, J. Mater. Res. **7**, 613 (1992).
[2] W. C. Oliver and G. M. Pharr, J. Mater. Res. **7**, 1564 (1992).
[3] W. W. Gerberich, J. C. Nelson, E. T. Lilleodden, P. Anderson, and J. T. Wyrobek, Acta Mater. **44**, 3585 (1996).
[4] S. Suresh, T.-G. Nieh, and B. W. Choi, Scr. Mater. **41**, 951 (1999).
[5] A. Gouldstone, H.-J. Koh, K.-Y. Zeng, A. E. Giannakopoulos, and S. Suresh, Acta Mater. **48**, 2277 (2000).
[6] Y. Shibutani and A. Koyama, J. Mater. Res. **19**, 183 (2004).
[7] W. D. Nix, Metall. Trans. A **20**, 2217 (1989).
[8] W. D. Nix, Mater. Sci. Eng., A **234-236**, 37 (1997).
[9] S. G. Corcoran, R. J. Colton, E. T. Lilleodden, and W. W. Gerberich, Phys. Rev. B **55**, R16057 (1997).
[10] J. D. Kiely and J. E. Houston, Phys. Rev. B **57**, 12588 (1998).
[11] J. A. Zimmerman, C. L. Kelchner, P. A. Klein, J. C. Hamilton, and S. M. Foiles, Phys. Rev. Lett. **87**, 165507 (2001).
[12] J. Li, K. J. Van Vliet, T. Zhu, S. Yip, and S. Suresh, Nature (London) **418**, 307 (2002).
[13] K. J. Van Vliet, J. Li, T. Zhu, S. Yip, and S. Suresh, Phys. Rev. B **67**, 104105 (2003).
[14] R. Smith, D. Christopher, S. D. Kenny, A. Richter, and B. Wolf, Phys. Rev. B **67**, 245405 (2003).
[15] Y. Mishin, D. Farkas, M. J. Mehl, and D. A. Papaconstantopoulos, Phys. Rev. B **59**, 3393 (1999).
[16] Y. Mishin, M. J. Mehl, D. A. Papaconstantopoulos, A. F. Voter,

and J. D. Kress, Phys. Rev. B **63**, 224106 (2001).
[17] C. L. Kelchner, S. J. Plimpton, and J. C. Hamilton, Phys. Rev. B **58**, 11085 (1998).
[18] G. Simons and H. Wang, *Single Crystal Elastic Constants and Calculated Aggregate Properties* (MIT Press, Cambridge, MA, 1977).
[19] S. Ogata, J. Li, and S. Yip, Science **298**, 807 (2002).
[20] K. L. Johnson, *Contact Mechanics* (Cambridge University Press, Cambridge U.K., 2003).
[21] C. J. Smithells, *Smithells Metals Reference Book*, 7th ed. edited by E. A. Brandes and G. B. Brook (Butterworth-Heinemann, London, 1992).
[22] J. Li, Modell. Simul. Mater. Sci. Eng. **11**, 173 (2003).
[23] T. Tsuru and Y. Shibutani, Modell. Simul. Mater. Sci. Eng. **14**, S55 (2006).
[24] T. Tsuru and Y. Shibutani (unpublished).